Adaptive QRS detection based on maximum A posteriori estimation

Börjesson, Per Ola; Pahlm, Olle; Sörnmo, Leif; Nygards, M.E.

Published in:
IEEE Transactions on Biomedical Engineering

DOI:
10.1109/TBME.1982.324901

1982

William R. Brody (M'66) was born in Stockton, CA, in 1944. He received the S.B. and S.M. degrees in electrical engineering from the Massachusetts Institute of Technology, Cambridge, and the M.D. degree and the Ph.D. degree in electrical engineering from Stanford University, Stanford, CA.

Following Internship and Residency at Stanford and the University of California, San Francisco, he joined the faculty at Stanford in 1977, where he is currently Associate Professor of Radiology and Electrical Engineering and Director of the Advanced Imaging Techniques Laboratory. His research interests include medical imaging and cardiovascular diagnosis.

Dr. Brody is a Fellow of the American College of Cardiology and an Established Investigator of the American Heart Association.

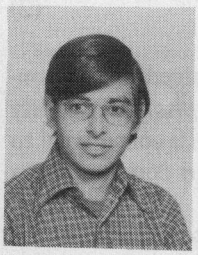

Barry P. Medoff (S'75) was born in New York, NY, in 1954. He received the B.S. degree (summa cum laude) from Yale University, New Haven, CT, in 1976, and the M.S. degree from Stanford University, Stanford, CA, in 1977.

In 1976 he was with the IBM Research Laboratory, San Jose, CA, and from 1977 to 1978 he was with the IBM Research Laboratory, Zurich, Switzerland, working on problems in image processing and halftone document reproduction. Since 1978 he has been with the Information Systems Laboratory, Department of Electrical Engineering, Stanford University, pursuing the Ph.D. degree. His research interests include medical imaging, signal processing, computer systems, and VLSI systems.

Mr. Medoff is a member of Phi Beta Kappa and Tau Beta Pi.

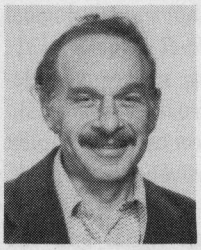

Albert Macovski (A'51-SM'56-F'76) received the B.E.E. degree from City College, New York, NY, in 1950, the M.E.E. degree from the Polytechnic Institute of Brooklyn, Brooklyn, NY, in 1953, and the Ph.D. degree in electrical engineering from Stanford University, Stanford, CA, in 1968.

From 1950 to 1957 he was a member of the Technical Staff at RCA Laboratories. From 1957 to 1960 he was an Assistant and then an Associate Professor at the Polytechnic Institute of Brooklyn. From 1960 to 1971 he was a Staff Scientist at the Stanford Research Institute. He served one year as a special NIH Fellow at the University of California Medical Center, San Francisco, and then joined the Stanford faculty as an Adjunct Professor and then Full Professor of Electrical Engineering and Radiology, his present position. His research has been in a variety of imaging systems including television, facsimile, holography, and interferometry. During the past five years he has been particularly involved with diagnostic imaging techniques in ultrasound and radiography.

Dr. Macovski is a Fellow of the Optical Society of America. In 1972 he received the IEEE Zworykin Award.

Adaptive *QRS* Detection Based on Maximum *A Posteriori* Estimation

PER OLA BÖRJESSON, MEMBER, IEEE, OLLE PAHLM, LEIF SÖRNMO, STUDENT MEMBER, IEEE, AND MATS-ERIK NYGÅRDS

Abstract—**A mathematical model for the occurrence of nonoverlapping pulse-shaped waveforms corrupted with colored Gaussian noise is considered for the purpose of *QRS* detection. The number of waveforms, the arrival times, amplitudes, and widths are regarded as random variables. The joint MAP estimation of all the unknown quantities consists of linear filtering followed by an optimization procedure. A class of filters is introduced which is easy to implement. The mismatching obtained by using this class for detection of model *QRS* complexes is investigated. The optimization procedure is time-consuming and is modified so that a threshold test is obtained. The model formulation with nonoverlapping waveforms leads to an "eye-closing" procedure covering a segment before as well as after an accepted event. Adaptivity of the detector is gained by utilizing past as well as future signal properties in determining thresholds for *QRS* acceptance.**

Manuscript received July 14, 1981; revised December 18, 1981. This work was supported in part by the Swedish Medical Research Council under Grant 14X-02872, the Swedish National Association Against Heart and Chest Diseases, and the Swedish Board for Technical Development.

P. O. Börjesson is with Facit AB, Svängsta, Sweden.

O. Pahlm is with the Department of Clinical Physiology, University Hospital, Lund, Sweden.

L. Sörnmo is with the Division of Telecommunication Theory, University of Lund, Lund, Sweden.

M.-E. Nygårds is with the Department of Medical Informatics, Linköping University, Linköping, Sweden.

I. Introduction

QRS detection in ambulatory ECG recordings presents a difficult problem. The signal is sometimes disturbed by nonstationary noise, and it is also subject to variations in amplitude due to time-varying impedance at the electrode-skin interfaces. Another problem arises from the fact that the morphology of "normal" *QRS* complexes may change during the time of recording due to changes in heart position relative to the electrodes. Such changes can be rapid, i.e., occur almost from one *QRS* complex to the next, due to rapid positional changes of the patient (e.g., a rapid change from recumbent to standing position). Further, *QRS* complexes of

0018-9294/82/0500-0341$00.75

quite different morphology, such as aberrantly conducted beats or beats of ventricular origin, may be intermingled with the "normal" *QRS* complexes.

During the last decade, the problem of detecting *QRS* complexes has been treated by several authors. Reliable *QRS* detection is of fundamental importance, whether the purpose is to locate tentative *QRS* complexes for further morphological analysis [1], [2], or to obtain a table of *R-R* intervals [3], [4]. Most recent detectors are intended for software implementation, which allows a more complex structure than realization in hardware. Since the *R* wave portion of the complex usually is easy to distinguish due to its relatively sharp peak, several algorithms incorporate simple slope criteria [5], [6]. Commonly, the peaks in the differentiated signal and the duration between these peaks are compared to thresholds, which are successively updated from past signal properties. To avoid power line interference and to reduce the influence of muscle artifacts and baseline shifts, simple digital filters are used [1], [7], [8]. Application of matched filters is discussed in [8], [9], where the problem of defining an accurate fiducial point is also considered.

Little theoretical work has been presented in the field of *QRS* detection. In the early seventies Haywood *et al.* considered a mathematical model for the purpose of detecting ventricular extrasystoles [10], [11]. In that work, the number of waveforms in the observation interval was known and the amplitude and arrival time were considered random quantities. We have in this paper started with a model formulation which has similarities to the problem of resolving different targets, as treated in radar theory [12]-[14]. In that case the object is to detect or estimate an unknown number of received waveforms and their arrival times.

In the first part of this paper, the signal model and the estimation procedure are presented. In Section IV, different aspects of the model, such as the effect of using filters mismatched to the input signal, are discussed in relation to ECG's. Further, the observation interval is delimited by means of two "significant" waveforms. By letting the properties of these waveforms determine the acceptance criteria within the interval, the detector adapts quickly to changes in *QRS* morphology. Also, such a delimitation is a means for utilizing both past and future signal properties. Since the detector is based on MAP estimation, the concepts "detector" and "estimator" are used interchangeably.

II. Joint Estimation of the Number of Waveforms and their Arrival Times

Signal Model and MAP Estimation

In this section we consider the following discrete-time model formulation; a finite sequence of variables $r(k), k = 1, 2, \cdots, N$, also denoted by the N-dimensional vector $\boldsymbol{r}$, is observed, containing an unknown number q of pulse-shaped waveforms, corrupted by additive, white Gaussian noise $w(k)$ with the spectral density $N_0/2$,

$$r(k) = \begin{cases} \sum_{i=1}^{q} B_i s(k - \theta_i, T_i) + w(k) & 1 \leqslant q \leqslant n \\ w(k) & q = 0. \end{cases} \tag{1}$$

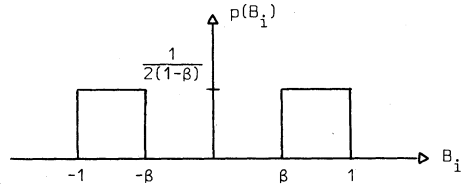

Fig. 1. The probability density for B_i.

Each waveform belongs to a known class of signals $[\sim s(k, \cdot)]$, but with unknown arrival time θ_i, amplitude B_i, and width T_i. The waveform $s(k, T_i)$ has a duration of less than D and is composed of two equal waveforms $v(k)$,

$$s(k, T_i) = \begin{cases} v(k) - v(k + T_i) & 0 \leqslant k \leqslant D - 1 \\ 0 & \text{otherwise.} \end{cases} \tag{2}$$

The parameters $q, \boldsymbol{\theta}$, and $\boldsymbol{T}$ are discrete-valued and $\boldsymbol{B}$, continuous-valued random variables. The joint *a priori* probability density is denoted by $p(q, \boldsymbol{\theta}, \boldsymbol{B}, \boldsymbol{T})$. Since q is constrained to the interval $0 \leqslant q \leqslant n$, it is sufficient with n components in each of the vectors $\boldsymbol{\theta}, \boldsymbol{B}$, and $\boldsymbol{T}$.

The arrival times $\theta_1, \theta_2, \cdots, \theta_q$ are separated by at least the distance D, i.e.,

$$|\theta_i - \theta_j| \geqslant D \quad \text{for} \quad i \neq j. \tag{3a}$$

Thus, the pulse-shaped waveforms are nonoverlapping. To guarantee that all waveforms are completely contained in the observation interval $1 \leqslant k \leqslant N$,

$$1 \leqslant \theta_i \leqslant N - (D - 1) \quad i = 1, \cdots, n. \tag{3b}$$

We require that q fulfills

$$q \leqslant n \leqslant \left\lfloor \frac{N - D}{2D - 1} + 1 \right\rfloor \tag{4}$$

where $\lfloor \cdot \rfloor$ denotes the integer part. With the constraint (4) it is possible to assume that q and $\boldsymbol{\theta}$ are independent. In our model all the random variables are independent, apart from an interdependence between the components of $\boldsymbol{\theta}$. Then the joint probability density can be written

$$p(q, \boldsymbol{\theta}, \boldsymbol{B}, \boldsymbol{T}) = \Pr(q) \Pr(\boldsymbol{\theta}) \prod_{i=1}^{n} p(B_i) \Pr(T_i) \tag{5}$$

for

$$(q, \boldsymbol{\theta}, \boldsymbol{B}, \boldsymbol{T}) \in \Omega^{(n)}_{q,\theta,B,T}$$

where $\Omega^{(n)}_{q,\theta,B,T}$ defines a sample space such that $p(q, \boldsymbol{\theta}, \boldsymbol{B}, \boldsymbol{T})$ is zero outside this space as follows. The probability for q waveforms,

$$\Pr(q) = \begin{cases} p_q & q = 0, 1, \cdots, n \\ 0 & \text{otherwise.} \end{cases} \tag{6}$$

The joint probability of the arrival times $\Pr(\boldsymbol{\theta})$ is uniform over those $\boldsymbol{\theta}$ which fulfill (3). The probability density $p(B_i)$ for the amplitude is "double-sided" uniform for $B_i \in [-1, -\beta]$ or $[\beta, 1]$; see Fig. 1. Finally, the probability $\Pr(T_i)$ is uniform for $T_i \in [\tau_1, \tau_2]$, where τ_1 and τ_2 are positive integers.

Based on the *a priori* knowledge $p(q, \boldsymbol{\theta}, \boldsymbol{B}, \boldsymbol{T})$ and the observed signal vector $\boldsymbol{r}$, we want to estimate the number of pulses q in the observation interval and their arrival times $\theta_1, \theta_2, \cdots, \theta_q$. To do this, we use the joint "maximum *a*

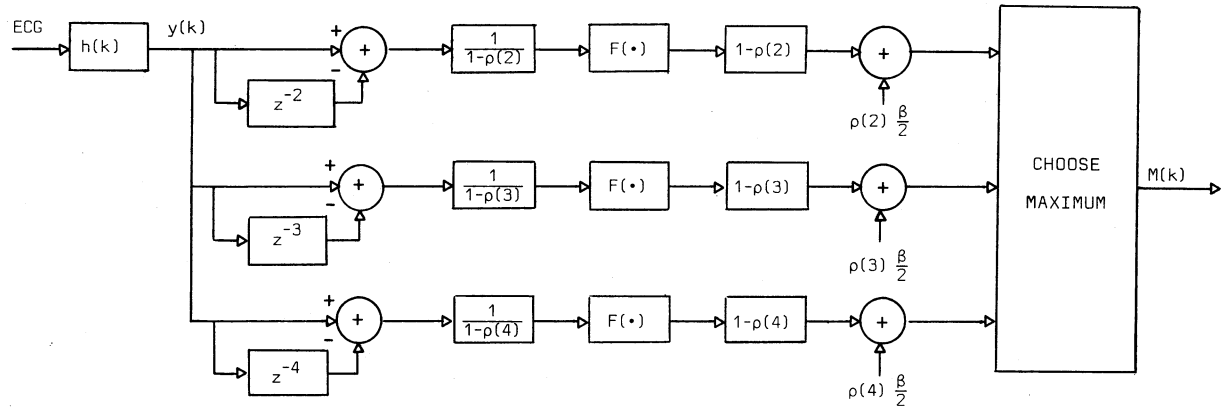

Fig. 2. Preprocessing of the ECG to calculate the function defined by (15). In the figure, the width T_i is constrained to the values 2, 3, or 4.

posteriori" (MAP) estimates of all the unknown parameters $q, \boldsymbol{\theta}, \boldsymbol{B}$, and $\boldsymbol{T}$. These joint MAP estimates are given by any $(\hat{q}, \hat{\boldsymbol{\theta}}, \hat{\boldsymbol{B}}, \hat{\boldsymbol{T}})$ that maximizes the log likelihood function [15],

$$V(\boldsymbol{r}, q, \boldsymbol{\theta}, \boldsymbol{B}, \boldsymbol{T}) = \frac{2}{N_0} \sum_{k=1}^{N} r(k) \sum_{i=1}^{q} B_i s(k - \theta_i, T_i) - \frac{1}{N_0} \sum_{k=1}^{N} \sum_{i=1}^{q} \left(B_i s(k - \theta_i, T_i) \right)^2 + \ln p(q, \boldsymbol{\theta}, \boldsymbol{B}, \boldsymbol{T}) \tag{7}$$

where the sums over i equal zero for $q = 0$. The first term in (7) can be obtained as a weighted sum of outputs from a linear, time-invariant filter with the impulse response

$$h_0(k) = \frac{v(-k)}{2E_v} \tag{8}$$

where E_v is the energy of $v(k)$, i.e., the sum of $v^2(k)$ over k. The output of the filter at the discrete time θ_i is given by the convolution sum

$$y(\theta_i) = \sum_{k=1}^{N} r(k) h_0(\theta_i - k). \tag{9}$$

In order to arrive at a convenient form for $V(\boldsymbol{r}, q, \boldsymbol{\theta}, \boldsymbol{B}, \boldsymbol{T})$, we introduce the following notation. The signal-to-noise ratio (SNR) for $B_i = 1$ is given by

$$d^2(T_i) = \frac{2}{N_0} \sum_{k=1}^{N} s^2(k, T_i) = d_0^2 (1 - \rho(T_i)) \tag{10}$$

where

$$d_0^2 = \frac{4E_v}{N_0} \tag{11}$$

and $\rho(T_i)$ is the normalized correlation sum for $v(k)$,

$$\rho(T_i) = \frac{1}{E_v} \sum_{k=0}^{D-1} v(k) v(k + T_i). \tag{12}$$

By means of the new notation and the *a priori* probabilities, the log-likelihood function is reduced to

$$V(\boldsymbol{r}, q, \boldsymbol{\theta}, \boldsymbol{B}, \boldsymbol{T}) = \sum_{i=1}^{q} d^2(T_i) \left[B_i \frac{y(\theta_i) - y(\theta_i - T_i)}{1 - \rho(T_i)} - \frac{B_i^2}{2} \right] + \ln p_q \tag{13}$$

for $(q, \boldsymbol{\theta}, \boldsymbol{B}, \boldsymbol{T}) \in \Omega^{(n)}_{q,\theta,B,T}$. In (13) we have omitted an additive constant.

We now maximize (13) with respect to $\boldsymbol{B}$, $\boldsymbol{T}$, and $\boldsymbol{\theta}$. First, we maximize over the vector-components in $\boldsymbol{B}$, $\boldsymbol{T}$, and $\boldsymbol{\theta}$ with index $q + 1 \leqslant i \leqslant n$, which is done by simply choosing these components in $\Omega^{(n)}_{q,\theta,B,T}$. In Appendix A, (13) is maximized with respect to B_i, resulting in a function $\hat{B}_i(\theta_i, T_i)$ which is then substituted for B_i in (13). The joint MAP estimates $\hat{q}, \hat{\boldsymbol{\theta}}, \hat{\boldsymbol{T}}$, and $\hat{\boldsymbol{B}}(\hat{B}_i = \hat{B}_i(\hat{\theta}_i, \hat{T}_i))$ are obtained by maximizing the log-likelihood function

$$V(\boldsymbol{r}, q, \boldsymbol{\theta}, \boldsymbol{T}) = \sum_{i=1}^{q} d^2(T_i) \beta \left[F\left(\frac{y(\theta_i) - y(\theta_i - T_i)}{1 - \rho(T_i)} \right) - \frac{\beta}{2} \right] + \ln p_q \tag{14}$$

over the sample space $\Omega^{(q)}_{q,\theta,T}$. The function $F(x)$ is given in Appendix A, see Fig. 7. Further, to eliminate T_i in an analogous manner, we introduce the function $M(\theta_i)$, defined by

$$M(\theta_i) = \max_{\tau_1 \leqslant T_i \leqslant \tau_2} \left[(1 - \rho(T_i)) F\left(\frac{y(\theta_i) - y(\theta_i - T_i)}{1 - \rho(T_i)} \right) + \rho(T_i) \frac{\beta}{2} \right]. \tag{15}$$

In this case we cannot find an explicit expression for the T_i that maximizes (15). The calculation of $M(\theta_i)$ is illustrated in Fig. 2 for $T_i \in [2, 4]$. Now, with (15) we can maximize

$$V(\boldsymbol{r}, q, \boldsymbol{\theta}) = d_0^2 \beta \sum_{i=1}^{q} \left[M(\theta_i) - \frac{\beta}{2} \right] + \ln p_q \tag{16}$$

over the sample space $\Omega^{(q)}_{q,\theta}$ to obtain the joint MAP estimates. When maximizing (16), which contains the quantities of primary interest q and $\boldsymbol{\theta}$, one could first look at a fixed q and determine those $\boldsymbol{\theta}$ that yield the maximum. Then, we take that q which gives the overall maximum.

Approximate MAP Estimation

The calculation of the estimates $(\hat{q}, \hat{\boldsymbol{\theta}})$ described in the previous section is tedious (particularly for large n), since it is a multidimensional optimization problem. We do not intend to find the optimum, but will be satisfied in finding the estimates $\tilde{q}, \tilde{\theta}_1, \cdots, \tilde{\theta}_{\tilde{q}}$ defined by the maximum $V_{\tilde{q}} = \max_{0 \leq q \leq n} V_q$. The function V_q is defined by the recursion

$$V_0 = 0$$

$$V_q = V(\boldsymbol{r}, q, \tilde{\theta}_1, \tilde{\theta}_2, \cdots, \tilde{\theta}_q) = \max_{\theta_q} V(\boldsymbol{r}, q, \tilde{\theta}_1, \tilde{\theta}_2, \cdots, \tilde{\theta}_{q-1}, \theta_q) \quad 1 \leq q \leq n \quad (17)$$

where $V(\boldsymbol{r}, q, \boldsymbol{\theta})$ in (16) from now on is redefined by omitting the additive constant $\ln p_0$. Thus in each step we only have to determine one parameter, $\tilde{\theta}_q$, which equally is obtained by maximizing the difference

$$\Delta V(\boldsymbol{r}, q, \theta_q) = V(\boldsymbol{r}, q, \tilde{\theta}_1, \tilde{\theta}_2, \cdots, \theta_q) - V(\boldsymbol{r}, q-1, \tilde{\theta}_1, \tilde{\theta}_2, \cdots, \tilde{\theta}_{q-1}) \quad 1 \leq q \leq n. \quad (18)$$

The maximum is denoted by Δ_q,

$$\Delta_q = V_q - V_{q-1} = \max_{\theta_q} \Delta V(\boldsymbol{r}, q, \theta_q) \quad 1 \leq q \leq n. \quad (19)$$

In terms of Δ_q, V_q can be written

$$V_q = \sum_{i=1}^{q} \Delta_i \quad 0 \leq q \leq n \quad (20)$$

with the sum defined as zero for $q = 0$.

By using (18) and (16) in (19) we obtain

$$\Delta_i = d_0^2 \beta \max_{\theta_i} [M(\theta_i) - \alpha_i(\theta_i)] \quad (21)$$

where

$$\alpha_i(\theta_i) = \frac{\beta}{2} + \frac{1}{d_0^2 \beta} \ln \frac{p_{i-1}}{p_i} \quad (22)$$

for $(\tilde{\theta}_1, \tilde{\theta}_2, \cdots, \tilde{\theta}_{i-1}, \theta_i) \in \Omega_\theta^{(i)}$. Equation (21) shows that any $M(\theta_i)$ which is larger than $\alpha_i(\theta_i)$ gives a positive contribution to V_q. With equal *a priori* probabilities for $q (p_i = 1/(n+1), i = 0, 1, \cdots, n)$, $\alpha_i(\theta_i)$ is independent of q and the procedure is analogous to a threshold test. In this case, we simply choose the maxima in turn starting with the largest one, while observing the cancelling operation of segments within the distance D from each picked maximum. This scheme is continued until no further maximum exceeding $\beta/2$ exists. Note that if $\tilde{q} = 1$, then $\hat{\theta}_1 = \tilde{\theta}_1$. Some examples of the approximate MAP estimation are found in Appendix B.

III. Modifications of the Model

From a mathematical model, a method has been developed for estimating the number of pulses in an observation interval and their arrival times. Only the white noise case was studied. We will here generalize the model to a continuous-time situation for band-limited waveforms corrupted with band-limited colored noise. A family of simple power spectra for the noise is used.

In general, estimation in colored noise is more complex than estimation in white noise. However, for an infinite observation interval and stationary noise, the increased complexity is essentially restricted to exchanging the matched filter. In the band-limited case, a discrete-time formulation leads to the same result as a continuous-time one, if the observed signal $r^c(t)$ (c denotes continuous time) is sampled with at least the Nyquist rate. We now allow continuous-valued arrival times θ_i for the waveforms in the observed signal (1). By constraining the estimator to produce only discrete-valued $\hat{\theta}_i$, a degradation in performance is obtained.

The impulse response of the matched filter will depend not only on the configuration of the input signal, but also on the power spectrum of the colored noise. Alternatively, if we specify a certain filter and a certain noise spectrum the filter will be matched to a certain input signal. We will investigate a class of filters with finite impulse response, described by two integer parameters.

Estimator for Sampled Signals Corrupted with Colored Noise

We assume that the noise is Gaussian with the power spectrum

$$R_n^c(f) \sim \begin{cases} \left| \dfrac{1 - be^{-j(\pi f/W)}}{1 - ae^{-j(\pi f/W)}} \right|^2 & |f| \leq W, \; 0 \leq a, b \leq 1 \\ 0 & |f| > W \end{cases} \quad (23)$$

where the bandwidth W is so large that the signal energy for $|f| \geq W$ is zero. The family of noise spectra (23) enables us to roughly model disturbances of low-pass character. Three spectra in this family are shown in Fig. 3 for various choices of the parameters a and b. Note that $a = b$ gives the white noise treated in Section II.

Despite the infinite observation interval (i.e., the observed signal $r^c(t)$ is given for $-\infty \leq t \leq \infty$) we restrict $\boldsymbol{\theta}$ to be such that the waveforms are completely contained in a finite interval, just as in Section II. Since $r^c(t)$ is band limited and given in an infinite interval, the sampled signal $r(k) = r^c(k/f_s)$ will contain the same amount of information (as long as the sampling rate $f_s > 2W$). Then, in the colored noise case the log-likelihood function is given by [15]

$$V(\boldsymbol{r}, q, \boldsymbol{\theta}, \boldsymbol{B}, \boldsymbol{T}) = \sum_{k=-\infty}^{\infty} r(k) \sum_{i=1}^{q} B_i g_0(\theta_i - k, T_i) - \tfrac{1}{2} \sum_{k=-\infty}^{\infty} \sum_{i=1}^{q} B_i s(k - \theta_i, T_i) \cdot \sum_{j=1}^{q} B_j g_0(\theta_j - k, T_j) + \ln p(q, \boldsymbol{\theta}, \boldsymbol{B}, \boldsymbol{T}). \quad (24)$$

Note that (24) differs from (7) not only in that the matched filter $s(k, T_i)$ is replaced by $g_0(k, T_i)$, but also that θ_i is now continuous-valued. The matched filter $g_0(k, T_i)$ is given by the inverse Fourier transform

$$g_0(k, T_i) = \mathcal{F}^{-1} \left\{ \frac{S^*(\nu, T_i)}{R_n(\nu)} \right\} = \int_{-1/2}^{1/2} \frac{S^*(\nu, T_i)}{R_n(\nu)} e^{j2\pi\nu k} \, d\nu \quad (25)$$

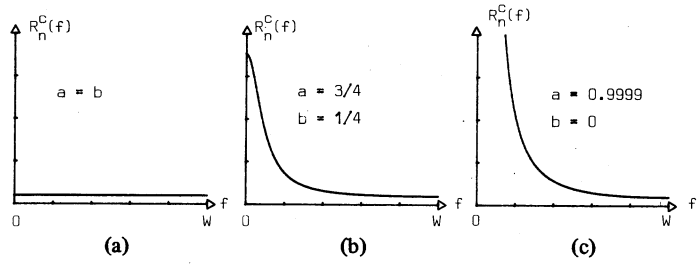

Fig. 3. Noise spectra for three choices of a and b.

where $S(\nu, T_i)$ is the Fourier transform of $s(k, T_i)$,

$$S(\nu, T_i) = \mathcal{F}\{s(k, T_i)\} = \sum_{k=-\infty}^{\infty} s(k, T_i)e^{-j2\pi\nu k} \tag{26}$$

and $R_n(\nu)$ is the power spectrum for the sampled noise. Since $f_s > 2W$

$$R_n(\nu) = f_s R_n^c(f_s\nu) \tag{27}$$

with $R_n^c(f)$ given by (23). For the purpose of utilizing the results in Section II, we will redefine some of the quantities defined there. Due to the colored noise situation, (8) is changed to

$$h_0(k) = \mathcal{F}^{-1}\left\{\frac{V^*(\nu)}{d_0^2 R_n(\nu)}\right\} \tag{28}$$

where d_0^2 is such that

$$d_0^2 = 2\int_{-1/2}^{1/2} \frac{|V(\nu)|^2}{R_n(\nu)}\,d\nu. \tag{29}$$

Furthermore, $\rho(T_i)$ in (12) is replaced by

$$\rho(T_i) = 2\sum_k v(k)h_0(T_i - k). \tag{30}$$

We neglect the energy outside the duration D of the waveform $s(k, T_i)$ and the matched filter $g_0(k, T_i)$. Then, with the quantities (25)-(30) inserted into (24), the estimator is almost the one in Section II. The difference is that θ_i in (24) is continuous-valued, so (28) should be evaluated for continuous k. The estimator could be implemented by using a number, P, of filters in parallel, $h_0(k)$, $h_0(k + 1/P), \cdots, h_0(k + (P-1)/P)$. For a sufficiently large P we have then implemented an estimator for continuous-valued θ_i. In the following we use $P = 1$, i.e., the estimator produces only discrete-valued $\hat{\theta}_i$. This choice leads to two types of errors.

1) An extra error in the estimate of the arrival time is introduced.

2) The maximal possible signal magnitude after the "matched" filter is reduced (loss in SNR).

The first error is at most equal to $1/(2f_s)$. The second error is investigated in the next section.

A Class of Filters

We will now treat the case when the filter $h_0(k)$ and the power spectrum of the colored noise in (27) are given. The matched filter $g_0(k, T_i)$ in (24) is then determined by (25), (28), and (2). Thus,

$$g_0(k, T_i) = d_0^2\{h_0(k) - h_0(k - T_i)\}. \tag{31}$$

Utilizing this filter and the power spectrum (27) in (25), we obtain a unique waveform $s(k, T_i)$ to which $g_0(k, T_i)$ is matched. Since the continuous-time signal is band limited, it is uniquely determined as

$$s^c(t, T_i) = \int_{-1/2}^{1/2} R_n(\nu)G_0^*(\nu, T_i)e^{j2\pi\nu f_s t}\,d\nu. \tag{32}$$

To evaluate (31) we specify the filter $h_0(k)$. We will here treat a class of filters for $h_0(k)$ defined by two integer parameters K(=1, 2, 3, or 4) and L(=0, 1, 2 or 3)

$$h_{KL}(k) = Z^{-1}\{(1 - z^{-K})(1 + z^{-1})^L z^D\} \tag{33}$$

where $Z^{-1}\{\,.\,\}$ is the inverse Z-transform. In the time domain, the first part $(1 - z^{-K})$ forms a difference between the input and the delayed input (K samples). For example, for $K = 1$ the result is the first-difference signal of the input. The second part $(1 + z^{-1})^L$ is a low-pass filter with decreased bandwidth for increased L. Finally, the factor z^D is included in the filter to fit the structure in Section II. When implementing the filter, z^D could be left out with the consequence that the output will be delayed by D samples. Filters within the structure (33) have been used in [1] and [7]. Using $h_{KL}(k)$ for $h_0(k)$ in (31) we obtain the filter

$$g_{KL}(k, T_i) = d_0^2\{h_{KL}(k) - h_{KL}(k - T_i)\}. \tag{34}$$

Since $h_{KL}(k)$ is antisymmetric, $g_{KL}(k, T_i)$ is symmetric. The signals $s^c(t, T_i)$ of Fig. 4 have been obtained by replacing $g_0(k, T_i)$ in (32) with $g_{KL}(k, T_i)$. Once K, L and the noise spectrum [a and b in (23)] have been chosen, the filter will be matched (apart from the first error) to the sampled versions of waveforms given by varying the parameter T_i (one time axis in the figure). In spite of the simple parametric structure of the filter $h_{KL}(k)$, we can model a fairly wide class of signals. One constraint is that only symmetric signals can be modeled. In the next section, we will further study the filters in the given class, when they are used on symmetric and antisymmetric sampled signals.

IV. Application of the Estimator to Sampled ECG's

In Sections II and III we have developed an estimator which works on a sampled signal. No reference was made to ECG's. Here, we will apply our estimator to ECG's sampled at $f_s = 100$ Hz. It is appropriate at this point to relate certain properties of the model that we used for determining the estimator to the corresponding ECG properties (see Table I).

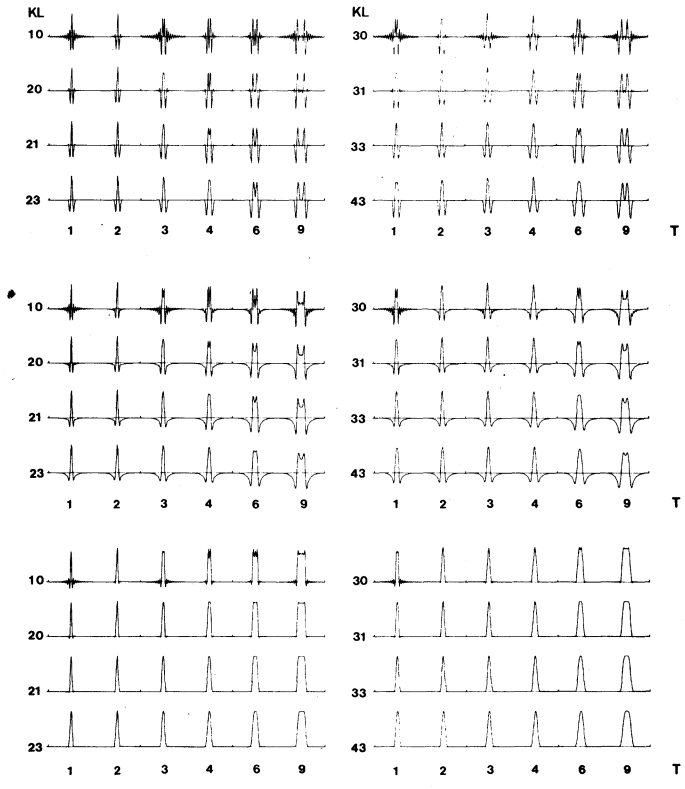

Fig. 4. Waveforms to which the filter $g_{KL}(k, T)$ is matched for three different noise spectra. (a) $a = b$. (b) $a = 3/4$, $b = 1/4$. (c) $a = 0.9999$, $b = 0$.

The discrepancy in property 1 is taken care of by prefiltering and sampling. The prefiltering implies that we lose some of the high-frequency characteristics of the signal. Since we can model low-frequency noise, cf. (23), important aspects of properties 2 and 3 can be taken care of, namely baseline wandering and T waves. These are in general more low-frequent than *QRS* complexes. High-frequency noise due to, e.g., muscular activity will be attenuated by the prefilter. Our model does not include any high-frequency noise above the white-noise level. In the subsections below we consider properties 4-6.

Assumptions of Rhythm

Most often *QRS* complexes are fairly regularly spaced along the time axis. Assuming a regular rhythm in the model would probably improve the performance in normal ECG's with sporadic artifacts. However, in our opinion, one should not impose a rigid structure on the timing of events since one of the most important qualities of a good *QRS* detector is to reliably detect *changes* in rhythm. These often are clinically important.

Our assumption of a uniform $\Pr(\boldsymbol{\theta})$ leads to an estimator which favors no particular locations of *QRS* complexes in the observation interval. However, we have postulated that they cannot overlap. Unequal *a priori* probabilities for the number of complexes in the observation interval $\Pr(q)$ may be used. This allows the estimator to favor a certain heart rate.

Mismatched Filters

In Section III we suggested a class of filters characterized by two integer parameters. Signals to which these filters could be matched were shown in Fig. 4. It is seen in this figure that,

TABLE I
PROPERTIES OF ECG'S VERSUS MODEL

	ECG	Model
1.	not strictly bandlimited	strictly bandlimited
2.	non-stationary, complex noise situation	bandlimited, coloured stationary Gaussian noise
3.	P waves, T waves and artifacts occur	P waves, T waves and artifacts not directly modelled
4.	rhythm most often regular	weak assumptions as regards rhythm
5.	wide class of waveforms	assumes waveforms of type depicted in Fig. 4.
6.	observed waveforms most probably have the same polarity	assumes positive and negative polarity with equal probability

in many cases, essential properties of *QRS* complexes are modeled. It is well-known from signal theory [15] that matched filters are often rather insensitive to moderate variations in signal and noise properties. In the present section, we want to study the reduction in performance that results from using filters in the given class ($h_{KL}(k)$) to input signals that are not matched to the filter. We will investigate some of the combinations of K and L used in Fig. 4. As input signals, we have chosen two model *QRS* complexes with variable widths, $s_I^c(t)$ and $s_{II}^c(t)$ given by

$$s_I^c(t) \sim e^{-t^2/2\sigma^2} \tag{35a}$$

$$s_{II}^c(t) \sim te^{-t^2/2\sigma^2}. \tag{35b}$$

Linear combinations of these waveforms have been used by some authors to describe essential characteristics of *QRS* complexes [1], [16], [17]. *QRS* waveforms with mono- and biphasic configurations can be modeled. The width is easily controlled by σ.

We have used the reduction in signal-to-noise ratio that results from mismatching as our measure of performance. We use the definition

$$\mathrm{SNR}\,(g(k)) = 10 \cdot {}^{10}\log \frac{\max\limits_{k} \left\{ \sum\limits_{l} s(l)g(k-l) \right\}^2}{\left\{ \int_{-1/2}^{1/2} |G(\nu)|^2 R_n(\nu)\, d\nu \right\}} \tag{36}$$

where $g(k)$ is the impulse response of any receiving filter and $s(k)$ is the input waveform under study, not necessarily in the class given by (2). The maximum SNR is obtained when $g(k)$ is matched to $s(k)$, i.e.,

$$\mathrm{SNR}_{\max} = 10 \cdot {}^{10}\log \int_{-1/2}^{1/2} \frac{|S(\nu)|^2}{R_n(\nu)}\, d\nu. \tag{37}$$

In our case the signal $s(k)$ is obtained by sampling one of the continuous time signals, given by (35)

$$s(k) = s_i^c\left(\frac{k-\epsilon}{f_s}\right) \tag{38}$$

where $|\epsilon| \leqslant \frac{1}{2}$. The filter $g(k)$ is in our case $g_{KL}(k, T_i)$, given by (34). For the corresponding reduction in SNR, given by the difference between (36) and (37), we use the notation $R(K, L, \epsilon, T_i)$. If, for given K, L, and ϵ, we could choose T_i such that $R(K, L, \epsilon, T_i) = 0$, (i.e., no mismatching), the filter $g_{KL}(k, T_i)$ would be matched to the input in the sense given by Sections II and III (unknown parameter T_i). For each K and L and each input signal under study the optimum T_i is used, i.e., we only use the maximum of $R(K, L, \epsilon, T_i)$ over T_i, which we denote

$$R(K, L, \epsilon) = 10 \cdot {}^{10}\log \max_{T_i} \frac{\max\limits_{k} \left\{ \sum\limits_{l} s(l)g_{KL}(k-l, T_i) \right\}^2}{\int_{-1/2}^{1/2} |G_{KL}(\nu, T_i)|^2 R_n(\nu)\, d\nu \int_{-1/2}^{1/2} \frac{|S(\nu)|^2}{R_n(\nu)}\, d\nu} \tag{39}$$

where $s(k)$ now is given by (38). The maximal reduction in SNR due to the choice of arrival time of the input signal is given by

$$R_{\max}(K, L) = \max_{|\epsilon| \leqslant 1/2} R(K, L, \epsilon) \tag{40}$$

which is our measure of mismatching. Even if this quantity is zero, another set of samples from the continuous-time waveform (another ϵ) will degrade the performance of the *KLT* filter, i.e., an extra error in the arrival time will occur. We measure this error as the difference

$$\Delta R(K, L) = R_{\max}(K, L) - \min_{|\epsilon| \leqslant 1/2} R(K, L, \epsilon). \tag{41}$$

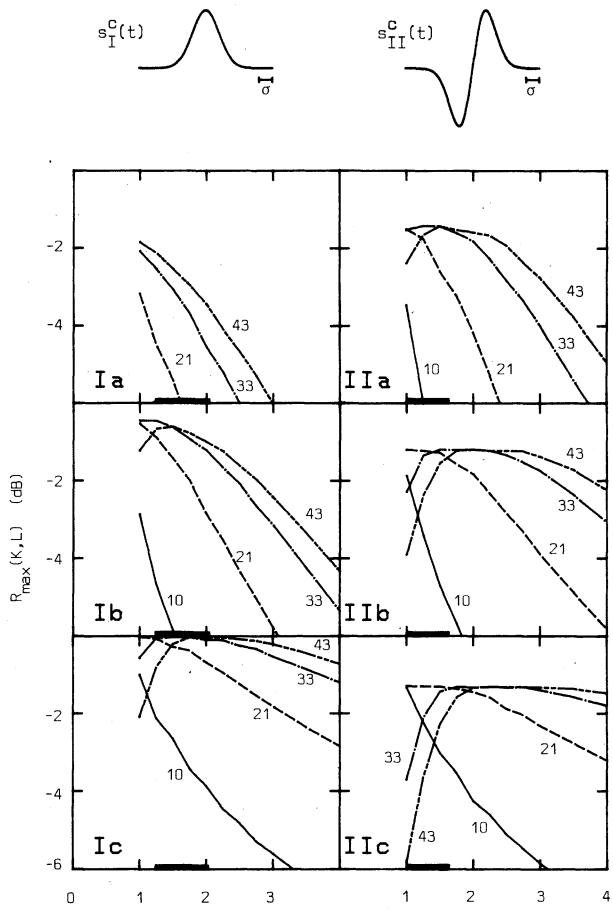

Fig. 5. Reduction in SNR due to mismatching, $R_{\max}(K, L)$, using the filter $g_{KL}(k, T)$ for the input signals $s_I^c(t)$ or $s_{II}^c(t)$ in the three different noise situations. $R_{\max}(K, L)$ is shown as a function of the width parameter σ. Diagrams Ia and IIa correspond to the noise spectrum with $a = b$, Ib and IIb to $a = 3/4$, $b = 1/4$, and Ic and IIc to $a = 0.9999$, $b = 0$. The two numbers at each curve are the filter parameters *KL*. The range of normal *QRS* width (0.06–0.1 s) is indicated by a broader line along the σ axis.

Fig. 5 shows $R_{\max}(K, L)$[1] for various σ and for the three noise spectra of Fig. 3. It is evident that the case when $K = 1, L = 0$ does not need further consideration. This is also indicated in Fig. 4, where many of the cases with $L = 0$ are not very similar to *QRS* complexes. For small σ ("normal" *QRS* width) and the colored noise situation [Fig. 5(b) and (c)] the best performance is seen for $s_I^c(t)$. The reason is that the receiver is matched to signals which are essentially monophasic (see Fig. 4 for small T_i). The antisymmetric signal $s_{II}^c(t)$ almost represents a "worst case" for the present filter structure, since the filter essentially "sees the main peak" of the input signal.

In the cases of Fig. 5, the reduction $\Delta R(K, L)$ was always less than 1.5 dB for signal I and 2.6 dB for signal II. Disregarding the case $K = 1, L = 0$, $\Delta R(K, L)$ was less than 1 dB for all cases. As expected $\Delta R(K, L)$ decreases with increasing σ. For $\sigma > 2$, $\Delta R(K, L)$ was less than 0.5 dB.

With the *KLT* filter and our assumption of a two-sided *a priori* probability density for the amplitude, the estimator can

[1]The optimization in (40) and (41) is approximately performed by varying ϵ in steps of $\frac{1}{30}$. Since the signals (35) are not band limited, aliasing will occur in (38). This means that $\mathrm{SNR}_{\max}$ in (37) will depend on ϵ. The greatest variation was only 0.05 dB.

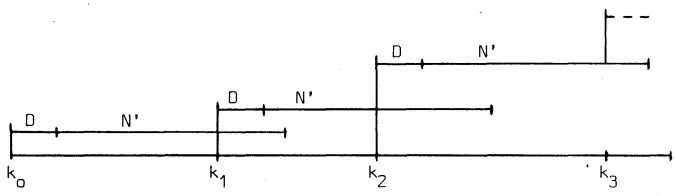

Fig. 6. Delimitation of the observation interval. The time k_0 denotes the arrival time of a type-event. The signal is inspected in the primary interval of length N' starting at $(k_0 + D)$. The next type-event is found at k_1. The detector now uses $(k_0 + D, k_1 - D)$ as an observation interval for the estimation procedure. Next, a new primary interval of length N' starts at $(k_1 + D)$ and the type-event is found at k_2 and so on.

"follow" changes in width and shape. Such changes may be due to position changes of the patient or to aberrant conduction and ventricular extrasystoles (VES's).

Delimitation of the Observation Interval

The estimator works in an observation interval of known length N. When applying the estimator to real ECG's, an observation interval must first be defined. In Section II it was also assumed that all the waveforms in the interval were completely contained in it. One approach to defining such an interval is to let two "significant" waveforms delimit it. If these waveforms, which we denote "type-events," are actually *QRS* complexes, an interval has been delimited which completely contains all *QRS* complexes in between (a certain time must elapse between two consecutive *QRS* complexes). To determine a type-event, the estimator is used in the same way as before (cf. Sections II and III), but the procedure is finished after estimating the first arrival time, which thus becomes the location of the new type-event. Now, the observation interval is of length N' $(>N)$ and starts at the "distance" D from the last detected type-event. The choice of this "primary" interval length N' depends on the environment in which the detector should work. If the interval is too short, it may contain nothing; if it is too long, the signal properties may have changed quite drastically. The detector was implemented with N' equal to 3 s. In real-time applications, e.g., in a CCU the length N' is upwards limited by the size of the data buffer, or by the maximum acceptable delay, without serious medical consequences.

From the type-events one could obtain an estimate of the maximal amplitude B_i and normalize the observed signal with it. This adapts the ECG amplitude to the model with the maximal amplitude of B_i equal to one. Also the parameters τ_1 and τ_2, which define $\Pr(T_i)$, could be estimated from the properties of the type-events. With this structure, the detector adapts quickly to the prevailing waveform, provided that liberal acceptance criteria are used in the selection of the type-events. After having determined the type-event, the *QRS* detector works in a noncausal way. Decisions based on signal properties of the past, as well as the future, seem more reliable to us than decisions based only on properties of the past. The delimitation and estimation processes are summarized in Fig. 6.

Look-Back for Prolonged R-R Intervals

An indication of where the detector may have missed a *QRS* complex is given by observing the sequence of estimated arrival times, or rather the lengths of the intervals between them (*R-R* intervals). For example, low amplitude extrasystoles may be hidden in a prolonged interval. To decide if an *R-R* interval is prolonged several methods could be used (e.g., [18]-[20]). One simple method is to compare each *R-R* interval to a running average of the preceding intervals. The interval of interest could be subject to a "look-back," i.e., letting the estimator look once more using a more generous choice of the parameters β, τ_1, and τ_2. Furthermore, the filtering could be performed with a different choice of filter parameters K and L, in order to find complexes with aberrant morphology. However, it should be emphasized that by including a look-back facility not only the probability of finding every *QRS* complex increases, but also the risk of detecting large *T* waves or noise/artifacts in prolonged intervals.

Computational Considerations

The calculation of MAP estimates, as described in the former part of Section II, is a time-consuming task. For monitoring of ambulatory ECG's, we have implemented a version which differs from the optimal one, but which requires a modest amount of computation. That version included the approximate way of finding estimates $\tilde{q}, \tilde{\theta}_1, \cdots, \tilde{\theta}_{\tilde{q}}$; see (17)-(22).

Furthermore, a "peak-picking" strategy is used for an approximate calculation of the function $M(\theta_i)$. This strategy is motivated by observing that the choice of the two points $y(\theta_i)$ and $y(\theta_i - T_i)$, see (15), in practice often coincides by simply picking two adjacent peaks in $y(k)$ with opposite sign. If the correlation $\rho(T_i)$ is zero for $\tau_1 \leqslant T_i \leqslant \tau_2$, then in most cases the peak-picking yields the estimates $(\tilde{q}, \tilde{\theta}_1, \cdots, \tilde{\theta}_{\tilde{q}})$ [21], [22].

V. Results and Discussion

Clinical experience from about 600 12-h recordings, and a study of the performance of our monitoring system as a whole indicate that the *QRS* detector works well in the clinical routine [23]. The performance of the detector has preliminarily been evaluated for a material consisting of several ECG's from different patients [21], [22]. We will discuss here some of the properties of the detector which were indicated by that study. At present, a more extensive evaluation of the detector is being carried through.

The false alarms that occurred were most often caused by the existence of tall and peaked *T* waves. Since their spectral properties differ little from those of the *QRS* complexes, it seems difficult to suppress such *T* waves by means of selective filtering. One way to make the *T* wave "harmless" is to increase the eye-closing period, i.e., the distance D in (3a). However, such an increase will be at the expense of missing early VES's [24]. In the implemented version, the distance D was equal to 0.16 s. A *QRS* detector described in [25] applies an eye-closing period after each detected *QRS* complex. Hopefully, our noncausal strategy will also reduce the number of false alarms in situations where an artifact immediately precedes a *QRS* complex, even for a short eye-closing period. Others claim that by transforming the differenced ECG signal by means of squaring, windowing, and averaging, it will yield a single positive peak for each *QRS* complex, while suppressing the *P* and *T* waves [26].

In situations of a gradual decrease in amplitude with no fast return to the previous level, the detector behaves very well.

This behavior is due to the idea of letting type-events delimit the observation interval. A price to be paid for the adaptivity of the detector is that small complexes, intermingled with very large-amplitude ones, may be missed. If such a situation occurs, the detector adapts itself to the properties of the large-amplitude complexes, i.e., these are chosen as type-events.

Some attempts have been made to theoretically analyze the performance of *QRS* detectors [27], [28]. Such an analysis is carried through in terms of the accuracy of a fiducial point in [28], where the detection algorithm consists of a filter and a single-level, dual-level, or peak detector. In our study, we have investigated the reduction in performance that results from using filters mismatched to the input signal. The results indicate that the loss in SNR when using a first-difference filter, i.e., $(K, L) = (1, 0)$, is unacceptable (see Fig. 6), while most other choices of K and L may be appropriate. In order to make the detector insensitive to disturbances such as high-frequency muscle noise or baseline shift/wandering, it was implemented with $(K, L) = (2, 1)$ which has a bandpass characteristic (center frequency 19.6 Hz).

Appendix A
Calculation of the Function $\hat{B}_i(\theta_i, T_i)$

Let us denote each term in the first sum on the right-hand side of (13) with $U(\theta_i, B_i, T_i)$. The value of this function is the contribution to the log-likelihood function for one "pulse" with the arrival time θ_i, amplitude B_i and width T_i. We shall maximize $U(\theta_i, B_i, T_i)$ with respect to B_i, resulting in a function $\hat{B}_i(\theta_i, T_i)$.

Completing the square in $U(\theta_i, B_i, T_i)$ yields

$$U(\theta_i, B_i, T_i) = \frac{d^2(T_i)}{2}\,[x^2 - (x - B_i)^2] \tag{A1}$$

for

$$(q, \boldsymbol{\theta}, \boldsymbol{B}, \boldsymbol{T}) \in \Omega^{(q)}_{q,\theta,B,T}$$

where

$$x = x(\theta_i, T_i) = \frac{y(\theta_i) - y(\theta_i - T_i)}{1 - \rho(T_i)} \tag{A2}$$

Since $\hat{B}_i(\theta_i, T_i)$ should be such that $\beta \leqslant |\hat{B}(\theta_i, T_i)| \leqslant 1$, the maximum over B_i is given by

$$U(\theta_i, \hat{B}_i(\theta_i, T_i), T_i) = \frac{d^2(T_i)}{2} \cdot \beta \left[F(x) - \frac{\beta}{2}\right] \tag{A3}$$

where the function $F(x)$ is shown in Fig. 7. Further, the corresponding function is given by

$$\hat{B}_i(\theta_i, T_i) = \begin{cases} \beta \cdot \operatorname{sign}(x)/|x| < \beta \\ x \quad \beta \leqslant |x| \leqslant 1 \\ 1 \cdot \operatorname{sign}(x)/|x| > 1. \end{cases} \tag{A4}$$

Note that for β-values close to one, the function $F(x) \simeq |x|$ for all x.

Appendix B
Three Examples of Approximate MAP Estimation

In order to reduce the computational load, we have introduced an approximate way of finding the estimates of the arrival times. The use of this estimation procedure is illustrated by means of three examples.

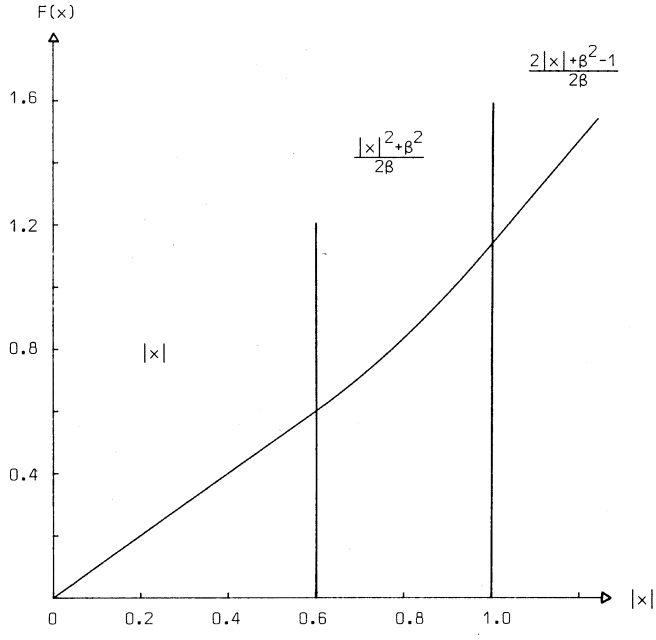

Fig. 7. The function $F(x)$ shown for $\beta = 0.6$.

Example 1

Let us consider the case when $n = 3$ and $p_i = 1/4, i = 0, 1, 2, 3$ (equal *a priori* probabilities for q). The function $M(k)$ used in (21) is shown in Fig. 8(a). The parameter D is shown in the same time scale. The width (above threshold $\alpha_i(\theta_i)$) of each peak in the output signal is smaller than D. Using the approximate MAP estimation described by (17)–(22) we get

$$\begin{aligned} &\Delta_0 = 0 \\ &\Delta_1 \sim M(k_2) - 0.40 = 0.55; \quad \tilde{\theta}_1 = k_2 \\ &\Delta_2 \sim M(k_3) - 0.40 = 0.50; \quad \tilde{\theta}_2 = k_3 \\ &\Delta_3 \sim M(k_4) - 0.40 = -0.10. \end{aligned} \tag{B1}$$

Using (B1) in (20) we get

$$\begin{aligned} &V_0 = 0 \\ &V_1 \sim 0.55 \\ &V_2 \sim 1.05 \\ &V_3 < V_2 \end{aligned} \tag{B2}$$

and thus

$$(\tilde{q}, \tilde{\boldsymbol{\theta}}) = (\hat{q}, \hat{\boldsymbol{\theta}}) = (2, k_2, k_3). \tag{B3}$$

The strategy is to pick the maxima, starting in turn with the largest one while observing the cancelling operation of segments within the distance D from each picked maximum. This scheme is continued until no further maximum exceeding $\beta/2$ exists. In this case, the result of the approximate strategy is *identical* to the optimum one.

Example 2

In this example, the *a priori* probabilities for q are unequal, $(p_0, p_1, p_2, p_3) = (1/8, 1/4, 1/2, 1/8)$, but with n still equal to 3 and $d_0^2\beta = 10 \cdot \ln 2$. The output is shown in Fig. 8(b).

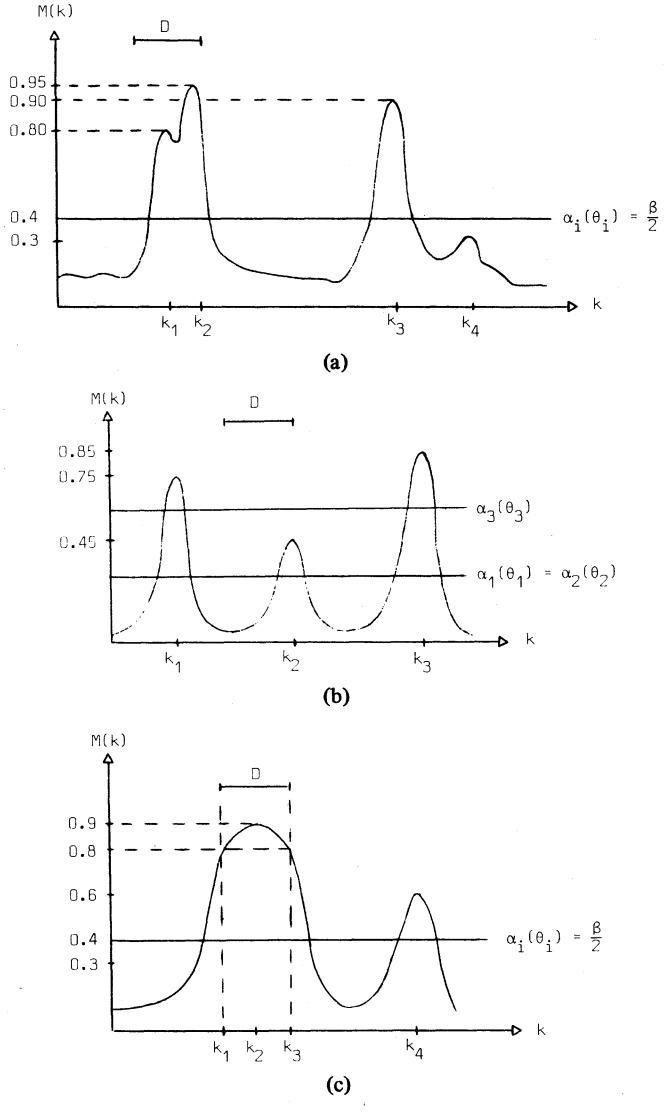

Fig. 8. A stylized example of the function $M(k)$ used in (21), for simplicity plotted as a continuous-time signal, and the threshold $\alpha_i(\theta_i)$ when the *a priori* probabilities (a) p_i are equal; (b) p_i are unequal; (c) p_i are equal and a wide peak occurs.

Calculating (20) we obtain

$$\Delta_0 = 0$$

$$\Delta_1 \sim M(k_3) - \left(0.4 + \frac{\ln 4/8}{d_0^2\beta}\right) = 0.55$$

$$\Delta_2 \sim M(k_1) - \left(0.4 + \frac{\ln 2/4}{d_0^2\beta}\right) = 0.45$$

$$\Delta_3 \sim M(k_2) - \left(0.4 + \frac{\ln 8/2}{d_0^2\beta}\right) = -0.15 \tag{B4}$$

and the estimate is

$$(\tilde{q}, \tilde{\boldsymbol{\theta}}) = (\hat{q}, \hat{\boldsymbol{\theta}}) = (2, k_3, k_1). \tag{B5}$$

The strategy is not so simple now as in Example 1, where the noncancelled peaks were compared only to a constant threshold. In the general case, we must calculate all the quantities V_q and choose the largest. Also in this case, the approximate strategy yields the same estimates as the optimum one.

Example 3

We consider $n = 6$ and $p_i = 1/7$ for $i = 0, 1, \cdots, 6$, but in this case the output signal contains a wide peak as shown in Fig. 8(c).

We sum up (20) to yield the "log-likelihood function" V_q,

$$V_q = d_0^2\beta \sum_{i=1}^{q} \max_{\theta_i} [M(\theta_i) - \alpha_i(\theta_i)]. \tag{B6}$$

Then for $d_0^2\beta = 1$ we get

$$V_0 = 0$$

$$V_1 = M(k_2) - 0.4 = 0.5$$

$$V_2 = V_1 + M(k_4) - 0.4 = 0.85$$

$$V_3 < V_2 \tag{B7}$$

and

$$(\tilde{q}, \tilde{\boldsymbol{\theta}}) = (2, k_2, k_4). \tag{B8}$$

In this case, the result of the approximate strategy differs from the optimum one. Equation (16) yields for

$$V(r, 0) = 0$$

$$V(r, 1, \theta_1) = M(k_2) - 0.4 = 0.5$$

$$V(r, 2, \theta_1, \theta_2) = M(k_1) + M(k_3) - 2 \cdot 0.4$$

$$= 0.8 > V(r, 1, \theta_1)$$

$$V(r, 3, \theta_1, \theta_2, \theta_3) = M(k_1) + M(k_3) + M(k_4) - 3 \cdot 0.4$$

$$= 1.0 > V(r, 2, \theta_1, \theta_2)$$

$$V(r, 4, \theta_1, \theta_2, \theta_3, \theta_4) < V(r, 3, \theta_1, \theta_2, \theta_3) \tag{B9}$$

and

$$(\hat{q}, \hat{\boldsymbol{\theta}}) = (3, k_1, k_3, k_4).$$

Note that k_1 and k_3 are not obtained from the peaks in the output signal.

References

[1] M.-E. Nygårds and J. Hulting, "An automated system for ECG monitoring," *Comput. Biomed. Res.*, vol. 12, pp. 181-202, 1979.
[2] C. N. Mead, K. W. Clark, G. C. Oliver, and L. J. Thomas, Jr., "Progress toward fully automated processing of ambulatory ECGs," *Proc. Comput. Cardiol.*, pp. 183-188, 1976.
[3] O. Pahlm, B. Jonson, O. Werner, K. Johansson, and K. Pettersson, "Computer-aided visual analysis of long-term ECG recordings," *Europ. Heart J.*, vol. 2, pp. 487-498, 1981.
[4] M. Okada, "A digital filter for the *QRS* complex detection," *IEEE Trans. Biomed. Eng.*, vol. BME-26, pp. 700-703, Dec. 1979.
[5] J. D. Coleman and M. P. Bolton, "Microprocessor detection of electrocardiogram R-waves," *J. Med. Eng. Tech.*, vol. 3, pp. 235-241, Sept. 1979.
[6] E. D. Gerlings, D. L. Bowers, and G. A. Pol, "Detection of abnormal ventricular activation in a coronary care unit," *Comput. Biomed. Res.*, vol. 5, pp. 14-24, 1972.
[7] W.A.H. Engelse and C. Zeelenberg, "A single scan algorithm for *QRS*-detection and feature extraction," *Proc. Comput. Cardiol.*, pp. 37-42, 1979.
[8] K. M. McClelland and J. M. Arnold, "A *QRS* detection algorithm for computerized ECG monitoring," *Proc. Comput. Cardiol.*, pp. 447-450, 1976.
[9] R. Dillman, N. Judell and S. Kuo, "Replacement of AZTEC by correlation for more accurate VPB detection," *Proc. Comput. Cardiol.*, pp. 29-32, 1978.

[10] L. J. Haywood, R. E. Kalaba, V. K. Murthy and J. M. Richardson, "A decision-theoretical approach to the detection of ECG abnormalities: I. Ventricular extrasystoles," *Math. Biosci.*, pp. 357–366, 1970.
[11] J. M. Richardson, L. J. Haywood, V. K. Murthy, and R. E. Kalaba, "A decision-theoretical approach to the detection of ECG abnormalities: II. Approximate treatment of the detection of ventricular extrasystoles," *Math Biosci.*, pp. 97–103, 1971.
[12] A. Zielinski, "Resolution of overlapping echo signals in sonar/radar systems," *IEEE Trans. Commun.*, vol. COM-27, pp. 1321–1326, Sept. 1979.
[13] J. A. Stuller, "Generalized likelihood signal resolution," *IEEE Trans. Inform. Theory*, vol. IT-21, pp. 276–282, May 1975.
[14] M. G. Lichtenstein and T. Y. Young, "The resolution of closely spaced signals," *IEEE Trans. Inform. Theory*, vol. IT-14, pp. 288–293, Mar. 1968.
[15] H. L. van Trees, *Detection, Estimation and Modulation Theory: Part I.* New York: Wiley, 1968.
[16] L. Sörnmo, P. O. Börjesson, M.-E. Nygårds, and O. Pahlm, "A method for evaluation of *QRS* shape features using a mathematical model for the ECG," *IEEE Trans. Biomed. Eng.*, vol. BME-28, pp. 713–717, Oct. 1981.
[17] J. Richardson, L. J. Haywood, V. K. Murthy, and G. Harvey, "A mathematical model for ECG waveforms and power spectra," *Math. Biosci.*, vol. 12, pp. 321–328, 1971.
[18] W. Gersch, E. Dong, Jr., and D. Eddy, "Cardiac arrhythmia classification: A heart-beat interval Markov chain approach," *Comput. Biomed. Res.*, vol. 4, pp. 385–392, 1970.
[19] H. Hristov, G. Astardjian, and C. Nachev, "An algorythm for the recognition of heart rate disturbances," *Med. Biol. Eng.*, vol. 9, pp. 221–228, 1971.
[20] E. T. Tsui and E. Wong, "A sequential approach to heart-beat interval classification," *IEEE Trans. Inform. Theory*, vol. IT-21, pp. 596–599, Sept. 1975.
[21] P. O. Börjesson, O. Pahlm, L. Sörnmo, and M.-E. Nygårds, "An adaptive *QRS*-detector based on maximum-a-posteriori estimation," Div. Telecommun. Theory, Univ. Lund, Tech. Rep. TR-137, Apr. 1980.
[22] P. O. Börjesson, "Data compression and signal estimation with application to digitized electrocardiograms," Ph.D. dissertation, Univ. Lund, May 1980.
[23] O. Pahlm, B. Jonsson, M. Lukes, and I. Ringqvist, "Conventional versus computer-aided interpretation of long-term ECG recordings," *Clin. Physiol.*, pp. 427–435, 1981.
[24] C. N. Mead, T. Ferriero, K. W. Clark, L. J. Thomas, Jr., J. R. Cox, Jr., and G. C. Oliver, "An improved ARGUS/H system for high-speed ECG analysis," *Proc. Comput. Cardiol.*, pp. 7–13, 1975.
[25] C. Pieper and L. J. Thomas, Jr., "*QRS* detection for the SICU," Biomed. Comput. Lab., St. Louis, MO, Monograph 222, Feb. 1974.
[26] I.S.N. Murthy and M. R. Rangaraj, "New concepts for PVC detection," *IEEE Trans. Biomed. Eng.*, vol. BME-26, pp. 409–416, July 1979.
[27] J. Fraden and M. R. Neumann, "*QRS* wave detection," *Med. Biol. Eng. Comput.*, vol. 18, pp. 125–132, Mar. 1980.
[28] G.J.H. Uijen, J.P.C. de Weerd and A.J.H. Vendrik, "Accuracy of *QRS* detection in relation to the analysis of high-frequency components in the electrocardiogram," *Med. Biol. Eng. Comput.*, vol. 17, pp. 492–502, July 1979.

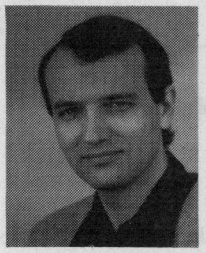

Per Ola Börjesson (S'70–M'80) was born in Sweden on September 8, 1945. He received the M.S. and Ph.D. degrees in electrical engineering from the University of Lund, Lund, Sweden, in 1970 and 1980, respectively.

From 1970–1972 he was employed at LM Ericsson working with theoretical aspects in radar and laser systems. From 1972–1980 he was a Teaching and Research Assistant at the Division of Telecommunication Theory, University of Lund. From 1979–1981 he was with the Department of Biomedical Engineering, Malmö General Hospital, Malmö, Sweden. He is currently employed at Facit AB, Svängsta, Sweden, working with the development of typewriters. His research interests include data compression and digital signal processing applied to ECG's, ultrasonics, and other acoustic signals.

Olle Pahlm was born in Sweden on March 15, 1944. He received the M.S. degree in electrical engineering and the M.D. degree from the University of Lund, Lund, Sweden, in 1970 and 1978, respectively.

From 1971 to 1977 he worked as a Research and Teaching Assistant at the Division of Telecommunication Theory, University of Lund. His doctoral thesis (Lund, 1980) treated computer-aided visual analysis of long-term ECG recordings. He is presently a resident at the Department of Clinical Physiology, University Hospital, Lund. His main research interests include computer processing of biomedical signals.

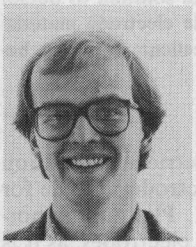

Leif Sörnmo (S'80) was born in Sweden on August 26, 1955. He received the M.S. degree in electrical engineering from the University of Lund, Lund, Sweden, in 1978.

He is presently a graduate student at the Division of Telecommunication Theory, University of Lund. His interests includes statistical signal processing and modeling of biological signals.

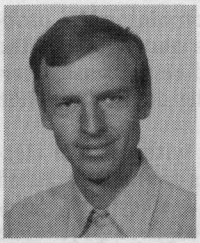

Mats-Erik Nygårds was born in Sweden on November 15, 1944. He received the M.S. degree in electrical engineering from the Royal Institute of Technology, Stockholm, Sweden, in 1969.

He is presently associated with the Department of Medical Informatics, Linköping University, Linköping, Sweden. His research interests are in biomedical signal processing and pattern recognition with application to ECG monitoring and ambulatory ECG analysis.